Acta Crystallographica Section B
Structural Science
ISSN 0108-7681
Editor: **Sander van Smaalen**

On the structural relations of malachite. II. The brochantite MDO polytypes

Frank Girgsdies and Malte Behrens

Acta Cryst. (2012). B**68**, 571–577

Acta Crystallographica Section B
Structural Science
ISSN 0108-7681

On the structural relations of malachite. II. The brochantite MDO polytypes

Frank Girgsdies* and Malte Behrens

Department of Inorganic Chemistry, Fritz-Haber-Institut der Max-Planck-Gesellschaft, Faradayweg 4-6, Berlin D-14195, Germany

Correspondence e-mail: girgsdie@fhi-berlin.mpg.de

Received 8 June 2012
Accepted 14 September 2012

The structural relation between malachite and the brochantite MDO (maximum degree of order) polytypes is discussed. It is demonstrated that the same building blocks which form the basis of brochantite polytypism also occur in malachite. The different arrangements of these building blocks in the two mineral structures are rationalized as a result of the different coordination geometries required by the respective non-metal atoms acting as linkers. The compound stoichiometries are discussed in light of a common structured formula scheme, in which pairs of H atoms can play a similar role as single non-H atoms. An overview on the occurrence of malachite-like building blocks in several other crystal structures is given.

1. Introduction

Both malachite, $Cu_2(OH)_2CO_3$, and brochantite, $Cu_4(OH)_6SO_4$, are secondary minerals formed in the oxidation zone of copper deposits and thus often occur together. The crystal structure of malachite has been investigated by Wells (1951), Süsse (1967) and Zigan *et al.* (1977). The latter study yields the space group $P2_1/a$, a = 9.502, b = 11.974, c = 3.24 Å, β = 98.75°, and was used for our structure discussion. The brochantite crystal structure was studied *e.g.* by Cocco & Mazzi (1959), Helliwell & Smith (1997) and Vilminot *et al.* (2006). The fact that brochantite is actually polytypic was established by Merlino *et al.* (2003), who discussed the order–disorder (OD) nature of brochantite and deduced that there are two possible MDO (maximum degree of order) polytypes, which was also demonstrated experimentally. The traditional brochantite structure corresponds to MDO_1 or brochantite-$2M_1$, with space group $P12_1/a1$ and the unit-cell parameters a = 13.140 (2), b = 9.863 (2), c = 6.024 (1) Å, β = 103.16 (3)°. The new MDO_2 structure (brochantite-$2M_2$) was refined in the space group $P2_1/n11$ with a = 12.776 (2), b = 9.869 (2), c = 6.026 (1) Å, α = 90.15 (3)°. Subsequently, the occurrence of brochantite-$2M_2$ was also reported from a different locality by Crichton & Müller (2008).

In some cases, structural or spectroscopic investigations on malachite and brochantite have been conducted by the same workers, or even published together. For example, Schmidt & Lutz (1993) investigated the hydrogen bonding in synthetic malachite and brochantite by IR and Raman spectroscopy, discussing their results in the context of the corresponding crystal structures. Both structures were depicted with their respective c axes as the viewing direction, but in different representation styles. Thus, the similarity between the two crystal structures was not quite obvious from the figures. Moreover, the authors briefly compared the brochantite structure to that of botallackite $Cu_2(OH)_3Cl$, rather than

Table 1
Comparison of unit-cell metrics (parameters rounded for convenience).

Malachite	Brochantite-2M_1	Brochantite-2M_2	Discrepancy†
$P12_1/a1$	$P12_1/a1$	$P2_1/n11$	
$a \sin\beta = 9.39$ Å	$b = 9.86$ Å	$b \sin\alpha = 9.87$ Å	6.6%
$b = 11.97$ Å	$a \sin\beta = 12.79$ Å	$a = 12.78$ Å	4.9%
$2c = 6.48$ Å	$c = 6.02$ Å	$c = 6.03$ Å	7.3%
$2V = 729$ Å^3	$V = 760$ Å^3	$V = 760$ Å^3	4.2%

† The discrepancy refers to the comparison of malachite *versus* brochantite-2M_1.

comparing brochantite and malachite with each other. Perchiazzi (2006) and Perchiazzi & Merlino (2006) showed figures of the malachite structure in comparison to the structures of related rosasite-type minerals. These figures have a remarkable resemblance to the brochantite structure depicted earlier by Merlino *et al.* (2003). However, we found no further indication that the authors were actually aware of this similarity. Eby & Hawthorne (1993) and Leonyuk *et al.* (2001) have treated the crystal chemical systematics of copper oxysalt structures. Both works include the structure of malachite but, surprisingly, do not cover brochantite. In summary, we are not aware of any previous work that would have subjected the crystal structures of the two minerals to a detailed comparison.

2. The topological similarity and structural relation between malachite and brochantite

A comparison of the malachite and brochantite structure projections along their respective *c* axes reveals a striking similarity (Fig. 1), although the stoichiometries of the two compounds do not suggest a particularly close relation. If the malachite formula is doubled to match the number of Cu atoms of the brochantite formula, *i.e.* $Cu_4(OH)_4(CO_3)_2$ *versus* $Cu_4(OH)_6SO_4$, neither the number of hydroxide groups nor that of oxyanions agree. Furthermore, it seems counter-intuitive that tetrahedral sulfate and trigonal planar carbonate groups could play a similar role in three-dimensionally extended structures. These might be the reasons why, despite the malachite and brochantite structures often being displayed along *c* in the literature, their similarity seems to have gone unnoticed so far. Fig. 1(*b*) reveals that the sulfate groups in brochantite are oriented in a special way: two of the four O atoms are ecliptic to each other when viewed along *c*, thus yielding a triangular projection of the sulfate tetrahedron. Table 1 demonstrates some degree of similarity of the unit-cell dimensions, although not particularly close. The best agreement is found for the direction corresponding to the malachite *b* axis, which still differs between malachite and brochantite-2M_1 by almost 5%.

As often described in the literature for the two structures separately, both are composed of double chains, or double ribbons, of edge-sharing CuO_6 octahedra running along the [001] direction. These double chains are interconnected *via* common corners into two-dimensional puckered layers. Thus, we can describe the building blocks which are common to malachite and brochantite as two-dimensionally infinite $^2_\infty[Cu_4O_{10}]$ moieties. The C or S atoms, respectively, can be interpreted as 'linkers' which join the two-dimensional building blocks into three-dimensionally extended networks (Fig. 2). Additionally, H atoms saturate the remaining valences and provide further cross-linking *via* hydrogen bonds (not shown). Thus, we may re-write the respective formulae as $^3_\infty\{^2_\infty[Cu_4O_{10}]C_2H_4\}$ for malachite and $^3_\infty\{^2_\infty[Cu_4O_{10}]SH_6\}$ for brochantite, reflecting the hierarchically nested construction

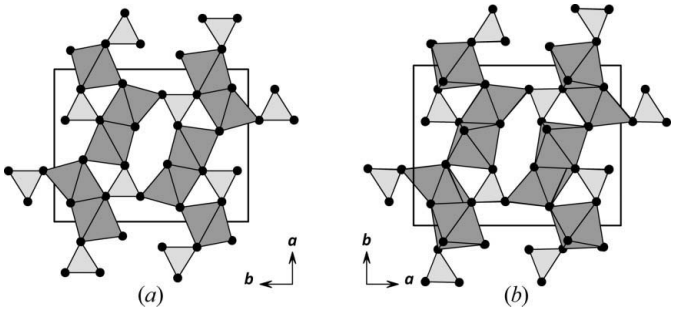

Figure 1
Comparison of the crystal structures of (*a*) malachite and (*b*) brochantite-2M_1, both viewed along their respective *c* axes. The structure of brochantite-2M_2 would look indistinguishable from brochantite-2M_1 in this representation. CuO_6 octahedra are displayed in dark gray, while CO_3 triangles and SO_4 tetrahedra are both shown in light gray. O atoms are represented as small black spheres at the corners of the polyhedra.

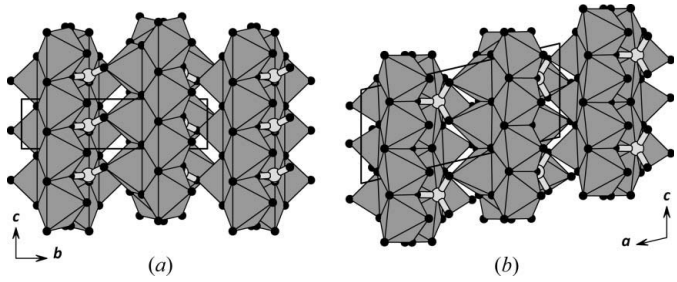

Figure 2
The crystal structure of (*a*) malachite viewed along *a* compared to (*b*) brochantite-2M_1 seen along *b*. While the CuO_6 moieties are again shown as dark gray octahedra, the carbonate and sulfate groups are now represented by light gray ball-and-stick models for better edge-on visibility of the carbonate and transparency of the sulfate groups.

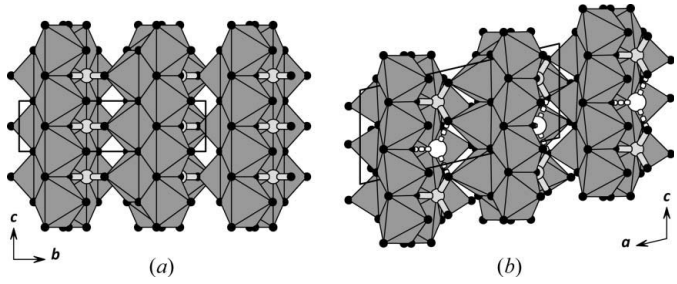

Figure 3
(*a*) Idealized orthorhombic malachite structure with *Pbam* symmetry compared with (*b*) brochantite-2M_1 containing tetrahedral voids. The tetrahedral voids are represented by white spheres, which are complemented by broken white 'bonds' to the surrounding O atoms (small black spheres) to emphasize the analogy between the tetrahedral vacancies and sulfate groups.

of the three-dimensionally extended crystal structures from common two-dimensionally infinite building blocks. In other words, we conceptually decompose the carbonate and sulfate groups into the non-metal linker atoms C and S, respectively, on the one hand, and the O atoms, which we consider to be part of the polyoxometalate building blocks, on the other hand. While such a conceptual decomposition might be counterintuitive from the chemical point of view, it proves to be helpful for the topological discussion.

Fig. 3 portraits the two structures in a modified way to guide the eye. As recently demonstrated, the crystal structure of malachite can be understood as a distortion derivative of a hypothetical orthorhombic structure, the 'Malachite–Rosasite Aristotype' (MRA; Girgsdies & Behrens, 2012). The MRA in turn is closely related to the structure of ludwigite $(Mg,Fe)_2FeO_2BO_3$ (Takéuchi *et al.*, 1950). In Fig. 3(*a*) we now depict the malachite structure in the idealized symmetry of the MRA, space group *Pbam*, revealing the general malachite topology more clearly. Fig. 3(*b*) shows that the brochantite structure contains tetrahedral voids between the $^2_\infty[Cu_4O_{10}]$ layers, which alternate with the tetrahedral sites occupied by sulfur. These unoccupied and occupied tetrahedra share common corners, thus forming infinite chains along [001].

Concerning the relation between the two structures in the third dimension, Fig. 3(*a*) shows that the length of the malachite *c* axis corresponds to the repeat distance of the carbonate groups along [001], as well as to the period of edge-sharing CuO_6 octahedra in this direction. The *c*-axis length of brochantite represents the repeat interval of the sulfate groups, which is in this case equivalent to a period of two CuO_6 octahedra (Fig. 3*b*). Thus, the *c* axis of brochantite corresponds to twice the malachite *c* axis, as expressed in Table 1. This is caused by the fact that tetrahedra occupied by sulfur alternate with tetrahedral vacancies, doubling the period which would result from the CuO_6 octahedra alone. Brochantite-2M_1 differs from brochantite-2M_2 in the way the third building block is arranged relative to the first two layers. Interchanging the unoccupied and occupied tetrahedra of the third block in brochantite-2M_1 seen in Fig. 3(*b*) would convert it into a section of brochantite-2M_2. If we regard all tetrahedra as equal, *e.g.* by filling them statistically with half a S atom each, we would obtain a smaller unit cell with half the brochantite *c* axis and higher symmetry (*Pbnm*). Such a hypothetical structure would be a superposition, or average, of the brochantite polytypes, thus serving as a model of the brochantite *family structure* discussed by Merlino *et al.* (2003).

The detailed relation between the malachite and brochantite arrangements of the $^2_\infty[Cu_4O_{10}]$ layers can be best explained with a simple, cartoon-like scheme (Fig. 4). The complex, puckered $^2_\infty[Cu_4O_{10}]$ layers are simplified as chains of dark gray octahedra in edge-on view. Carbon and sulfur are shown as light gray spheres. In malachite, symbolized by Fig. 4(*a*), two C—O bonds of each carbonate group are connected to one building block, while the third one establishes the link to the adjacent block (*cf.* Fig. 1*a*). This third C—O bond is removed in Fig. 4(*b*), detaching the building blocks from each other. In Fig. 4(*c*) every second block is shifted by half a period. This brings the C atoms at equal height between two tips of CuO_6 octahedra from the neighboring block, resulting in an approximately tetrahedral coordination, as shown in Fig. 4(*d*). While Fig. 4(*d*) is chemically implausible if interpreted as a 'tetrahedral carbonate' structure, it can be regarded as a sketch of the brochantite family structure instead. Brochantite-2M_1 is symbolized by Fig. 4(*e*), with sulfur-occupied tetrahedra alternating with tetrahedral vacancies symbolized by white, broken line spheres (*cf.* Fig. 3*b*). An interchange of occupied and unoccupied tetrahedra in the third block leads to Fig. 4(*f*), representing brochantite-2M_2. Finally, Fig. 4(*g*) depicts the block sequence of brochantite-2M_2 more clearly by showing an alternative section of the same arrangement as Fig. 4(*f*).

3. The local geometry around the linker groups

A point which has not been explained so far is how triangular carbonate and tetrahedral sulfate groups can both function as linkers between the $^2_\infty[Cu_4O_{10}]$ layers. For the planar carbonate group, this is geometrically more simple. Fig. 1(*a*) shows that two corners of the carbonate triangle are connected to one $^2_\infty[Cu_4O_{10}]$ block, while the third one establishes the

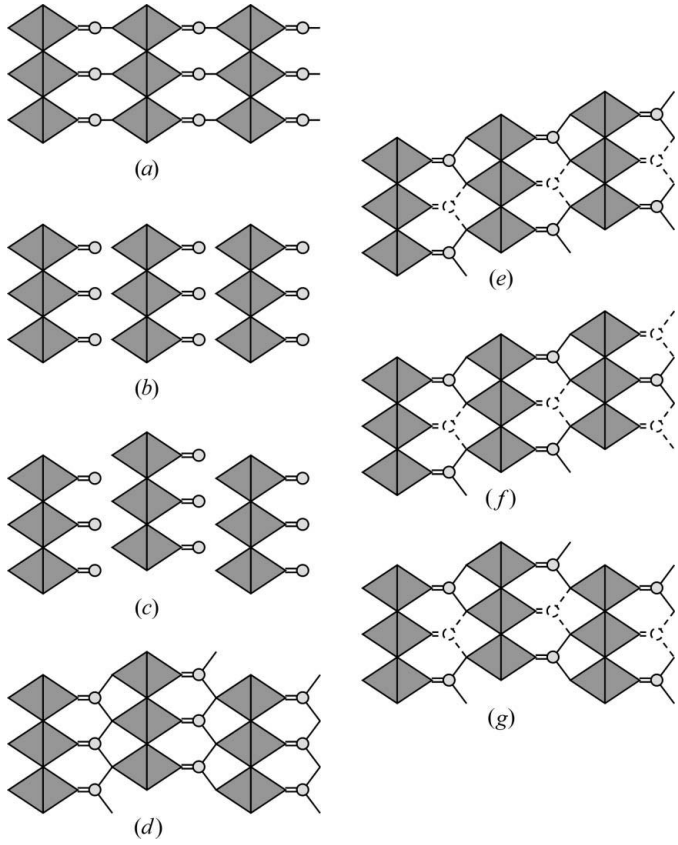

Figure 4
Cartoon-like sketch of the relation between the malachite and brochantite structures. (*a*) Symbolizes malachite in analogy to Fig. 3(*a*), while (*e*) corresponds to brochantite-2M_1 as seen in Fig. 3(*b*). (*a*)–(*d*) illustrate the virtual transformation of the malachite lattice into the brochantite family structure, while (*e*)–(*g*) depict different possible brochantite arrangements (see text for details).

connection to the neighboring block. Thus, the gape of one O—C—O angle (O···O distance 2.24 Å) has to be compatible with the shape of the $^2_\infty[Cu_4O_{10}]$ blocks (Fig. 5*a*, left), while the connection to the neighboring block (Fig. 5*a*, right) does not impose additional geometric restrictions. Two main factors provide sufficient flexibility of the building blocks. Firstly, the corner-sharing connection between the double ribbons of CuO_6 octahedra can act as a 'hinge' along [001], allowing some variation of the chelating gape, or puckering amplitude, of the $^2_\infty[Cu_4O_{10}]$ layers. Secondly, the Jahn–Teller distortion typical for the CuO_6 octahedra adds further flexibility, as the elongated axis can be positioned in three alternative orientations for each octahedron, leading to various possible combinations. The same two arguments also hold for the brochantite structures, *i.e.* one O—S—O angle of the sulfate tetrahedron (O···O = 2.42 Å) is also compatible with the geometry of a single $^2_\infty[Cu_4O_{10}]$ block (Fig. 5*b*, left). However, an additional criterion to be met now is that the gape of the opposite O—S—O angle has to match the tip-to-tip distance between two successive CuO_6 octahedra of a neighboring building block (O···O = 2.45 Å; Fig. 5*b*, right).

An analysis of the local geometry around the carbonate and sulfate linkers in malachite and brochantite confirms that the variable orientation of the long axial Cu—O bonds is an important factor. In brochantite, one sulfate O atom is μ^3 bridging between three Cu atoms, one is μ^2 bridging, while the remaining two are attached to only a single Cu atom each (Fig. 5*b*). All these connections involve only long, axial Cu—O bonds. In this respect, brochantite resembles many other copper oxysalts. It is worth noticing here that the double ribbons of edge-sharing CuO_6 octahedra in malachite and brochantite can be interpreted as slices of a two-dimensionally infinite brucite-like layer. Such layers are found in botallackite $Cu_2(OH)_3Cl$ and related $Cu_2(OH)_3L$ compounds, *e.g.* rouaite and gerhardtite $Cu_2(OH)_3NO_3$. In all these examples, the μ^3 attachment of the ligand L is realised *via* three axial Cu—O bonds, like in brochantite. In contrast, the carbonate O atoms in malachite are involved in both long axial and short equatorial Cu—O bonds. The μ^3 attachment features two short and one long bond, the μ^2 connection one of each, and the third O atom only a single short Cu—O bond (Fig. 5*a*), thus demonstrating a slight preference for the shorter equatorial bonds. We believe that the different distribution of the Jahn–Teller elongated bonds has probably helped obscuring the topological similarity between malachite and brochantite.

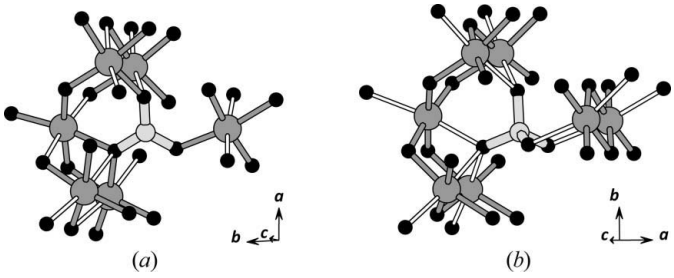

Figure 5
Local geometry around the linker groups (light gray): (*a*) carbonate in malachite and (*b*) sulfate in brochantite-2M_1. The axial bonds of the Jahn–Teller elongated CuO_6 octahedra (dark gray) are emphasized in white. Black spheres represent O atoms.

4. The role of the H atoms

So far, we have mostly neglected the role of the H atoms in the crystal structures of malachite and brochantite. The approximate location of H atoms in the respective crystal structures can easily be deduced chemically: every O atom which is not connected to a C or S linker atom must host one H atom. In malachite, all H atoms are thus associated with the 'channels' running along [001] which are apparent in the top view shown in Fig. 1(*a*). As discussed in an earlier contribution (Girgsdies & Behrens, 2012), the centers of these channels contain octahedral spaces, which are occupied with metal atoms in the ludwigite structure family (during the reviewing of this manuscript it was brought to our attention that the malachite–ludwigite relation has actually been discussed before by Belov, 1976). In order to emphasize the channel region we can rewrite the formula of a generalized ludwigite $M_3O_2BO_3$ in the form $M_2[M]^{channel}O_2BO_3$ (it should be noted that there is no simple relation between this topological notation and the distribution of different elements M and valences in the ludwigite structure type; thus we use the symbol M for all metal atoms irrespective of oxidation state). In the malachite-rosasite family $M_2(OH)_2CO_3$, the octahedral channel sites are associated with 'pairs' of H atoms, correspondingly yielding the notation $M_2[H_2]^{channel}O_2CO_3$. Consequently, we had concluded that the relation between the two structure families involves a formal correspondence between pairs of hydrogen sites and 'additional' metal sites in the channels: $[H_2]^{channel}_{malachite/rosasite} \leftrightarrow [M]^{channel}_{ludwigite}$ (Girgsdies & Behrens, 2012). While Fig. 1(*b*) reveals the existence of similar channels in brochantite, it is important to note that the brochantite channels do not contain octahedral sites due to the shift of the $^2_\infty[Cu_4O_{10}]$ channel 'walls' against each other along *c*. Four of six H atoms in brochantite $Cu_4(OH)_6SO_4$ are located within these channels. The remaining two, however, are associated with the tetrahedral voids which alternate with the sulfate tetrahedra along the *c* axis (Fig. 3*b*). Consequently, these tetrahedral 'vacancies' in brochantite are not really vacant, but again host 'pairs' of H atoms. In analogy to the hydrogen-pair *versus* metal substitution formulated previously for the malachite–ludwigite relation, we can now formalize a hydrogen-pair *versus* linker atom substitution for the relation between brochantite and malachite, *i.e.* $[H_2]^{linker} \leftrightarrow [X]^{linker}$. Here, X either represents every second malachite C atom if the two crystal structures are compared, or the brochantite S atom if the occupation pattern along the chains of corner-sharing tetrahedra within brochantite is discussed.

5. The malachite-like building block as a structural submotif in ludwigite and beyond

We have shown that malachite (Fig. 1*a*) and brochantite (Fig. 1*b*) share topologically identical $^2_\infty[Cu_4O_{10}]$ building blocks. Building blocks of the same type are also present in the

Table 2
Interpretation of compounds containing malachite-like building blocks according to the common formula scheme $\langle channel\rangle_2[M_4Y_{10}]\langle linker\rangle_2$.

The notation $\{H_2\}$ represents formal 'pairs' of H atoms, which are counted like single non-H atoms.

Conventional formula	Channel sites	Malachite-like framework	Linker sites	Linker geometry
$Cu_2(OH)_2CO_3$ (×2)	$\{H_2\}_2$	$[Cu_4O_{10}]$	C_2	Trigonal planar
$Cu_4(OH)_6SO_4$	$\{H_2\}_2$	$[Cu_4O_{10}]$	S $\{H_2\}$	Tetrahedral
$(Mg,Fe)_2FeO_2BO_3$ (×2)	$(Mg,Fe)_2$	$[(Mg,Fe)_2Fe_2O_{10}]$	B_2	Trigonal planar
$Mg_2Al_2O_5$ (×2)	$(Mg_{0.8}Al_{0.2})$ Al	$[(Mg_{0.3}Al_{0.7})_4O_{10}]$	Mg_2	Trigonal prismatic
$Ca_{0.76}In_{2.84}S_5$ (×2)	In_2	$[In_2(In_{0.84})_2S_{10}]$	$(Ca_{0.76})_2$	(Capped) trigonal prismatic
$NaTi_2Al_5O_{12}$	Na $\{AlO_2\}$	$[Ti_2Al_2O_{10}]$	Al_2	Tetrahedral

rosasite structure type, where some or all Cu atoms are replaced with other divalent metals. Furthermore, these blocks occur in the ludwigite $(Mg,Fe)_2FeO_2BO_3$ structure type as a sub-motif (Belov, 1976; Girgsdies & Behrens, 2012). As the crystal structure of ludwigite would remain three-dimensionally extended even without the boron linker atoms, the recognition of malachite-like $^2_\infty[M_4O_{10}]$ 'layers' as main constituents is of course purely conceptual (Fig. 6*a*).

Fig. 6(*b*) displays the high-pressure phase $Mg_2Al_2O_5$, which is formed during pressure-induced decomposition of $MgAl_2O_4$ (Enomoto *et al.*, 2009). In contrast to the ludwigite structure with its trigonal planar boron linker atom geometry, the magnesium linker atoms here have a trigonal prismatic environment resulting from a shift by half an octahedron period along the *c* axis relative to the building blocks. $Mg_2Al_2O_5$ demonstrates that the linker role is neither limited to non-metal atoms nor to trigonal planar and tetrahedral geometries. Furthermore, it is one of the few examples in which malachite-like building blocks occur in a crystal structure composed exclusively of main group elements.

The crystal structure of $Ca_{0.76}In_{2.84}S_5$ (Eisenmann & Hofmann, 1991; Fig. 6*c*) essentially looks like a blown-up version of $Mg_2Al_2O_5$ (Fig. 6*b*). The topology is almost identical, but all dimensions are expanded because of the larger atoms in $Ca_{0.76}In_{2.84}S_5$. A slight difference lies in the coordination geometry of the calcium linker atom. It is displaced from the center towards one of the faces of the trigonal prism, approaching a seventh S atom and reaching a sevenfold coordination. Thus, the actual geometry is capped trigonal prismatic. Nevertheless, Fig. 6(*c*) shows it as trigonal prismatic for better comparability, with the connection to the seventh ligand displayed as an 'additional' bond. $Ca_{0.76}In_{2.84}S_5$ is another rare case containing only main group elements and the only non-oxysalt with malachite-like building blocks that we are aware of.

All of the above examples follow a general composition scheme which may be denoted as $\langle channel\rangle_2[M_4Y_{10}]\langle linker\rangle_2$ (Table 2). Formally, the scheme can also be applied to $NaTi_2Al_5O_{12}$ (Mumme & Wadsley, 1967) if we re-write the formula as $Na\{AlO_2\}[Ti_2Al_2O_{10}]Al_2$, assigning two of the 12 O atoms to the channel region rather than the building block framework. The structure of $NaTi_2Al_5O_{12}$ (Fig. 6*d*) is slightly more complex than the previous examples and best compared with the ludwigite type (Fig. 6*a*). Metrically, $NaTi_2Al_5O_{12}$ is expanded along the *b* axis relative to ludwigite. This expansion is connected to two specific features in the atomic arrangement. Firstly, one of the two different channel sites is occupied by sodium, with a coordination environment best envisioned as an octahedron strongly elongated along one of its threefold axes, approximately parallel to *b*. Secondly, the other channel site hosts aluminium, accompanied by two extra O atoms. The latter are integrated into the polyhedral lattice in such a way that the orientation of the resulting AlO_6 octahedra at the channel sites differs from the ludwigite situation. Furthermore, the extra O atoms make the connection between the linker atoms and neighboring building blocks one step longer. Thus, a hybrid situation is achieved, in which the tetrahedral linker geometry resembles the brochantite case, but without the shift of adjacent building blocks along the *c* axis. In other words, the insertion of the extra O atoms near the second channel site introduces an offset which compensates the shift of the building blocks, which would otherwise be required by the tetrahedral linker geometry. In contrast to brochantite, all tetrahedral linker sites in $NaTi_2Al_5O_{12}$ are filled with non-H atoms, resulting in infinite chains of corner-sharing AlO_4 tetrahedra along [001].

All the crystal structures discussed above form a small but well defined subset of the large group of 3*n* Å wallpaper

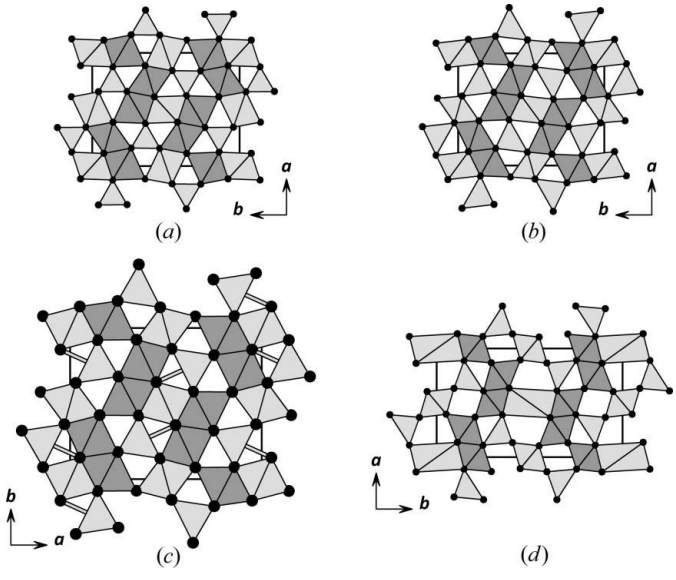

Figure 6
Further crystal structures containing malachite-like building blocks: (*a*) ludwigite, (*b*) $Mg_2Al_2O_5$, (*c*) $Ca_{0.76}In_{2.84}S_5$ and (*d*) $NaTi_2Al_5O_{12}$. Octahedra of the malachite-like framework are shown in dark gray, linker- and channel-site polyhedra in light gray. O and S atoms are represented by small and large black spheres, respectively. All structures are drawn to a common scale. Some unit-cell origins have been shifted relative to the originally published coordinates for comparability.

structures (Moore & Araki, 1974; Grice *et al.*, 1999) if we define it liberally. While Moore & Araki (1974) stated that the cations should occur either in triangular or octahedral coordination, we also need to allow other coordinations which have a triangular *projection* down the 3*n* Å axis (trigonal prismatic or tetrahedral in certain orientations). Among the 3*n* Å wallpaper structures, the closest relative of our malachite-like structures is probably the warwickite $(Mg,Ti,Al,Fe)_2OBO_3$ structure type (Takéuchi *et al.*, 1950). Inside the warwickite structure the typical topology of the malachite-like building block can be identified as a sub-motif (supplementary material, Fig. S1[1]). While the $^2_\infty[M_4O_{10}]$ layers found in malachite, brochantite and ludwigite are separated by channel and linker sites, they are fused to each other *via* shared O atoms into a three-dimensionally infinite $^3_\infty[M_4O_8]$ framework in warwickite. This 'condensation' reduces the number of O atoms in the generalized formula unit M_2OBO_3 (warwickite type) *versus* $M_3O_2BO_3$ (ludwigite type). As the 'interlayer space' is diminished while the number of linker sites stays the same, the corresponding reduction by one metal atom *M* per formula unit can be ascribed to the loss of the channel sites. The retention of the malachite-like building block dimensions during this 'condensation' is reflected in the very similar *a* and *c* axes of ludwigite and warwickite, while the collapse of the 'interlayer space' results in a *ca* 3 Å shorter *b* axis in warwickite.

Another point worth mentioning is that diorthosilicates may have structures which are analogous to orthoborates (see *e.g.* Belov, 1976). In such cases the di-tetrahedral Si_2O_7 group assumes the linker role in place of a stacked pair of triangular BO_3 groups along the 3*n* Å direction. Some well known examples for such structure pairs are jaffeite (or synthetic TSH) *versus* fluoborite, and cuspidine *versus* warwickite. Due to the length of the Si—O—Si bonds, diorthosilicates require an expansion of the wallpaper axis from 3*n* Å to *ca* (3.6–3.8)*n* Å. As a consequence, the chains of edge-sharing MO_6 octahedra need to be expanded correspondingly to match, which means that such diorthosilicates typically contain larger (*i.e.* Ca-sized rather than Mg-sized) cations on the octahedral sites. Due to its analogy to warwickite, condensed malachite-like building blocks can also be recognized in the cuspidine $Ca_4(F,OH)_2(Si_2O_7)$ structure (Smirnova *et al.*, 1955). However, we are neither aware of a silicate analogue of ludwigite, nor of any other silicate structure that would contain 'isolated' $^2_\infty[M_4O_{10}]$ layers of malachite-like topology.

6. Summary and conclusions

We have demonstrated that the crystal structures of malachite $Cu_2(OH)_2CO_3$ and brochantite $Cu_4(OH)_6SO_4$ are closely related to each other. Both contain topologically identical building blocks $^2_\infty[Cu_4O_{10}]$ which are interconnected by non-metal linker atoms into three-dimensionally extended structures. In contrast to the trigonal planar carbonate linker geometry in malachite, the tetrahedral sulfate groups in brochantite require that adjacent building blocks are shifted relative to each other by half a CuO_6 period. Furthermore, only every second linker site along [001] is occupied with sulfur, thus doubling the *c* axis. The combination of these factors results in different stacking possibilities for subsequent building blocks, leading to the brochantite polytypism.

Malachite-like building blocks are also present in the rosasite structure type and not limited to divalent copper. Furthermore, they occur in the ludwigite structure type and a few other related structures, as a sub-motif inside the three-dimensionally extended oxometalate frameworks. The same building principle is even realised in at least one chalcogenide, $Ca_{0.76}In_{2.84}S_5$. Thus, the malachite-like building block, though not very widespread, demonstrates its versatility across several chemical borders, including transition metal carbonates, sulfates and borates, and main group metal oxides and sulfides. All compounds discussed can be described with a common structured notation $\langle channel\rangle_2[M_4Y_{10}]\langle linker\rangle_2$. In this formal scheme, 'pairs' of H atoms $\{H_2\}$ assume the same role as single non-H atoms on channel or linker sites. Hence, this notation finally allows us to translate the structural similarity between malachite and brochantite into the correspondingly similar formulae $\{H_2\}_2[Cu_4O_{10}]C_2$ and $\{H_2\}_2[Cu_4O_{10}]S\{H_2\}$, respectively.

This work would have been impossible without online access to ICSD for WWW, provided by the Max Planck Society, and the *Jmol* visualization feature included. Robert Schlögl is acknowledged for his continuous support and fruitful discussions.

References

Belov, N. V. (1976). *Ocherki po strukturnŏi mineralogii (Essays on Structural Mineralogy)*. Moscow: Nedra.
Cocco, G. & Mazzi, F. (1959). *Period. Mineral.* **28**, 121–149.
Crichton, W. A. & Müller, H. (2008). *Powder Diffr.* **23**, 246–250.
Eby, R. K. & Hawthorne, F. C. (1993). *Acta Cryst.* B**49**, 28–56.
Eisenmann, B. & Hofmann, A. (1991). *Z. Kristallogr.* **197**, 165–166.
Enomoto, A., Kojitani, H., Akaogi, M., Miura, H. & Yusa, H. (2009). *J. Solid State Chem.* **182**, 389–395.
Girgsdies, F. & Behrens, M. (2012). *Acta Cryst.* B**68**, 107–117.
Grice, J. D., Burns, P. C. & Hawthorne, F. C. (1999). *Can. Mineral.* **37**, 731–762.
Helliwell, M. & Smith, J. V. (1997). *Acta Cryst.* C**53**, 1369–1371.
Leonyuk, L., Maltsev, V., Babonas, G.-J., Szymczak, R., Szymczak, H. & Baran, M. (2001). *Acta Cryst.* A**57**, 34–39.
Merlino, S., Perchiazzi, N. & Franco, D. (2003). *Eur. J. Mineral.* **15**, 267–275.
Moore, P. B. & Araki, T. (1974). *Am. Mineral.* **59**, 985–1004.
Mumme, W. G. & Wadsley, A. D. (1967). *Acta Cryst.* **23**, 754–758.
Perchiazzi, N. (2006). *Z. Kristallogr.* Suppl. **23**, 505–510.
Perchiazzi, N. & Merlino, S. (2006). *Eur. J. Mineral.* **18**, 787–792.
Schmidt, M. & Lutz, H. D. (1993). *Phys. Chem. Miner.* **20**, 27–32.
Smirnova, R. F., Rumanova, I. M. & Belov, N. V. (1955). *Zapiski Vserossiĭskogo mineralogicheskogo obshchestva (Proceedings of the Russian Mineralogical Society)* **84**, 159–169.
Süsse, P. (1967). *Acta Cryst.* **22**, 146–151.
Takéuchi, Y., Watanabé, T. & Ito, T. (1950). *Acta Cryst.* **3**, 98–107.

[1] Supplementary data for this paper are available from the IUCr electronic archives (Reference: BP5044). Services for accessing these data are described at the back of the journal.

Vilminot, S., Richard-Plouet, M., André, G., Swierczynski, D., Bourée-Vigneron, F. & Kurmoo, M. (2006). *Dalton Trans.* pp. 1455–1462.
Wells, A. F. (1951). *Acta Cryst.* **4**, 200–204.
Zigan, F., Joswig, W. & Schuster, H. D. (1977). *Z. Kristallogr.* **145**, 412–426.